Pulsar Profiles and the q-Gaussian and q-BWF Line Shapes

(Article begins on next page)

01 August 2024

Pulsar Profiles and the q-Gaussian and q-BWF Line Shapes

Amelia Carolina Sparavigna

Department of Applied Science and Technology, Polytechnic University of Turin, Italy

Email: amelia.sparavigna@polito.it

Torino, June 2, 2024

The EPN Database of Pulsar Profiles contains data provided by several generous researchers. Data are proposed by means of a web plotting tool. However, the pulsar profiles can be also obtained from the database in plain text format and therefore they can be easily used to test fitting procedures. Literature reports pulsar profile fits made by means of Gaussian line shapes. Here we propose the use of the q-Gaussian functions, which are generalizing the Gaussian functions. Since the observed profiles are also asymmetric, we propose the use for fitting of the q-BWF functions too. These functions are generalizing the Breit-Wigner-Fano line shapes, with the Breit-Wigner factor substituted by the q-exponential function. The q-exponential was proposed by Constantino Tsallis in 1988 for his generalization of Boltzmann-Gibbs statistics. Some preliminary fitting examples are here shown, of pulsar profiles from the EPN Database.

Keywords: Pulsar profiles, Profile decomposition, q-Gaussian Tsallis lines, Breit-Wigner-Fano line shape, q-BWF line shape.

Introduction

In a recent study about the radio pulsar emission-beam configurations (Wahl et al., 2023), the researchers used a Gaussian approach to fit the pulsar profiles for recovering the parameters relevant to their geometrical models. The Gaussian fitting procedure was made according to Kramer, 1994, and Kramer et al., 1994. In Wahl et al. and Kramer et al., we find that the pulsar profiles seem consisting of several Gaussian features. Consequently, a relevant problem that we must consider in the pulsar profile analysis is the choice of the method that we use for the decomposition. This is the same problem that we meet in the analysis of the Raman spectra, that is, their decomposition in several spectral components. In the case of Raman spectroscopy, it is well-known that the decomposition depends on the number of components and on the used line-shapes, usually in the form of Lorentzian, Gaussian and Voigt profiles (Ferrari and Robertson, 2000, Meyer, 2005). In 2023, I proposed for Raman spectroscopy a generalization of these profiles in the form of q-Gaussian line shapes. A q-Gaussian is a function based on the Tsallis q-form of the exponential function (Umarov et al., 2008). This generalized exponential is characterized by a q-parameter, and when q is equal to 2, we have the Lorentzian function. If q is close to 1, we have a Gaussian function (this is the reason why this Tsallis function is also known as "q-Gaussian"). For values of q between 1 and 2, we have a bell-shaped function with power-law tails ranging from the Gaussian to the Lorentzian behavior. As I have shown on many occasions, the q-Gaussian is suitable for fitting Raman spectra in a proper manner (see the discussion proposed in SSRN and the SERS cases, for instance).

In the case of pulsar profiles, as in the case of Raman spectra, the peaks are often asymmetric. The q-Gaussians, like Gaussian, Lorentzian and Voigt functions, are symmetric. To fit an asymmetric profile, the usual approach is to use more than one component or to split the line-shape into two parts, characterized by different parameters. For instance, a split-Lorentzian function is a Lorentzian line-shape with independent width parameters for the left and the right parts. However, a different approach to asymmetry exists and it is that based on the Breit-Wigner-Fano line shape. Let us write the BWF(x) function as follow:

$$\mathrm{BWF}(x) = C \frac{\left[1 - \xi \gamma^{1/2}(x - x_o)\right]^2}{\left[1 + \gamma(x - x_o)^2\right]}$$

When asymmetry parameter ξ is zero, the BWF function becomes a Lorentzian function. Parameter x_o is the center of the line. We can use the q-exponential to generalize the BWF (see also Appendix), and turn BWF into a q-BWF function:

$$q\text{-BWF}(x) = C\left[1 - \xi\gamma^{1/2}(q-1)^{1/2}(x-x_o)\right]^2 \left[1 + (q-1)\gamma(x-x_o)^2\right]^{1/(1-q)}$$

Comparing BWF and q-BWF, it is easy to see that the Lorentzian factor is substituted by the q-exponential. Please consider that in literature about Fano resonance (Bianconi, 2003) the parameter ξ is often given by $1/q$ (with an opposite sign). Here q is indicating the q-parameter related to the Tsallis statistics generalizing the Boltzmann-Gibbs statistics (Tsallis, 1988).

We have obtained good results with q-Gaussians and also with the q-BWF functions in Raman spectroscopy. Confident in the results from spectroscopy, here we start applying the q-Gaussians and the q-BWF functions to the decomposition of the pulsar profiles. The data we consider are from the EPN (European Pulsar Network) Database of Pulsar Profiles, which contains profiles provided by several generous researchers. Data are proposed by means of a web plotting tool. However, the pulsar profiles can be also obtained in the plain text format and therefore they can be easily used to test fit procedures. We could use Gaussian functions, such as in literature, but here we prefer to demonstrate that we can easily use the q-Gaussians for decomposing the pulsar profiles. In the case of evident asymmetry, the q-BWF functions are available too. For showing the decomposition, let us use Fityk software (Wojdyr, 2010). Fityk is a curve fitting and data analysis application, free and open source. It can perform a Levenberg-Marquardt algorithm, among other best fit algorithms. The function of merit is the weighted sum of squared residuals (WSSR), also called chi square. Fityk has several built-in functions but allows to execute a script with user-defined functions (see in the Appendix how we can define in Fityk q-Gaussian, split-q-Gaussian and q-BWF functions).

The decomposition is the first part of the problem. The second part is that of using the parameters obtained from decomposition into the geometrical specific models (see for instance Wahl and coworkers, 2023). Here we start investigating the decomposition by means of q-Gaussians and q-BWF functions of the pulsar profiles, giving some preliminary examples regarding profiles from the large database represented by EPN. Before showing decompositions, let us understand how many components we need to use.

Components of the pulsar profiles

About the physics of the pulsar emission, a review has been proposed by Harding, 2017. "Over the last fifty years since the discovery of pulsars, our understanding of where and how pulsars emit the radiation we observe has undergone significant revision. The location and mechanisms of high-energy radiation are intimately tied to the sites of particle acceleration. The evolution of emission models has paralleled the development of increasingly more sensitive telescopes, especially at high energies" (Harding, 2017).

Different models exist regarding the emission. One of the models is that based on the geometry of core/double cone beams, where two concentric conal beams exist around the central core beam. At p.6 of Joanna Rankin' presentation at Goddard Pulsar Workshop, an image shows how up to five components can be originated in a pulsar profile. In her publication of 2022, Rankin explains that the "Canonical pulsar average profiles are observed to have up to five components (Rankin, 1983). This places an important constraint on the emission-beam topology and underlies the conception of the core/double-cone beam model as originally proposed by Backer (1976)". According to this model, we have two major categories of pulsar profiles, "depending on whether core or conal emission components are dominant at about 1 GHz. Prominent core components occur in single (S_t) profiles consisting of an isolated core component, in core-cone triple (T) profiles with a core component flanked by a pair of outriding conal components, or in five-component (M) profiles where the central core component is flanked by both an inner and outer pair of conal components" (Rankin, 2022). "By contrast, entirely conal profiles include those with a single conal (S_d) component, double profiles (D) consisting of a pair of conal components (occasionally with a weak core component in-between), or conal triple (cT) or quadruple (cQ) profiles where the sightline encounters both conal beams. Outer conal component pairs tend to have an increasing separation with wavelength, whereas inner conal pairs tend to have more constant separations. Also important to these profile classes is single-pulse phenomenology" (Rankin, 2022).

Let us consider what told by Baker in 1975: "We are led by the observations and beam models … to hypothesize

the following criteria for inspecting pulsar radiation". Baker proposed five criteria, here in the following we report the first one. "The averaged beam pattern is a hollow-cone, perhaps with a pencil beam in the canter, which revolves around the rotation axis. The observer is randomly oriented with respect to the rotation axis at an angle θ_0 and the cone axis is either randomly oriented or randomly aligned with respect to the rotation axis at an angle θ_m. The average waveforms, or profiles, for several observer orientations are given in Figure 1 [by Baker, see here the sketch 1] which gives a schematic of the proposed beam geometry".
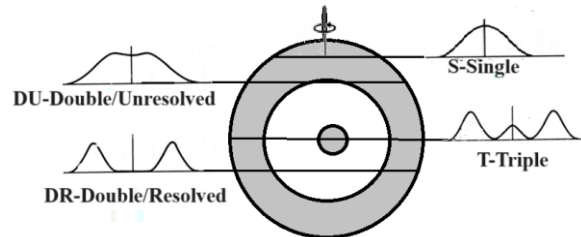
Sketch 1: This sketch is illustrating the Figure 1 in Baker, 1975. In the cone+core model, we have a maximum of three peaks.
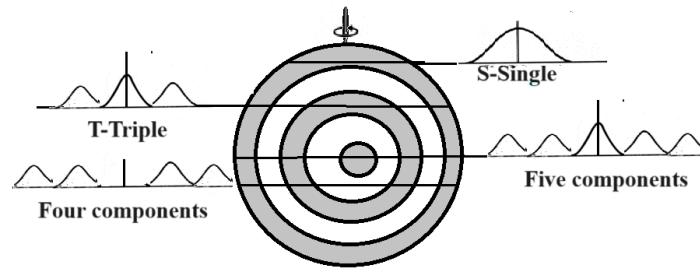
Sketch 2: Here a simple representation of a double-cone+core model. Note please that the figure in the slide by Rankin at p.6 the distribution in the rings is not depicted as an unbroken whole. It is a "carousel" of subbeams.

However, "two contrasting phenomenological models to explain the observed pulse shapes" exists. They are shown in Fig. 5 by Beskin et al., 2015. "The "core and cone" model, proposed by Rankin [Rankin, 1983], depicts the beam as a core surrounded by a series of nested cones. Alternatively, the "patchy beam" model, championed by Lyne and Manchester [Lyne & Manchester, 1988, Han & Manchester, 2001], has the beam populated by a series of randomly distributed emitting regions. Further work in this area, particularly in trying to quantify the variety of pulse shapes (number of distinct components and the relative fraction that they occur) is necessary to improve our understanding of the fraction of sky covered by the radio pulsar emission beam" (Beskin et al., 2015). Another model, proposed by Wang et al. in 2016, is the Fan Beam Model: "The whole radio beam may consist of several sub-beams, forming a fan-shaped pattern. When only one or a few flux tubes are active, the fan beam becomes very patchy. This model differs essentially from the conal beam models in the respects of beam structure" (Wang et al., 2016).

As previously told, we have the large EPN database to analyze, so let us here give some preliminary examples.

J1133—6250/1440 - Let us start from a profile that looks like that of a <u>Raman spectrum of graphene oxide</u>. We have two peaks. For them, let us use two q-BWF functions, because the components look asymmetric. Data are available at the following link: <u>https://psrweb.jb.man.ac.uk/epndb/#qmlg95/J1133-6250/qmlg95_1440.epn</u>, EPN database under the Creative Commons Attribution 4.0 International license. Data are courtesy by Guojun and coworkers, 1995.
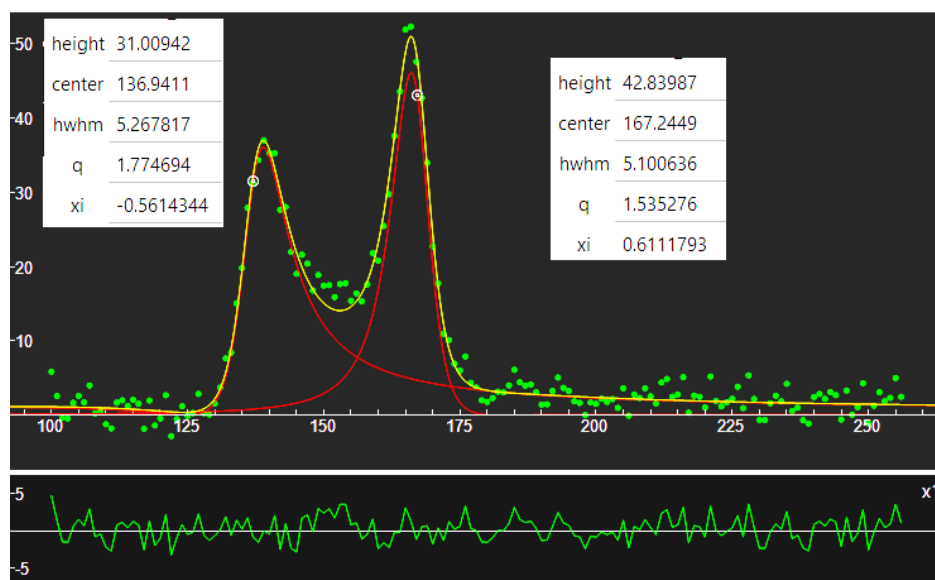

Fig.1: The image is giving a screenshot of Fityk. The parameters of the two used q-BWFs (red lines) are given in the figure. The sum of the two components is given in yellow, the data in green. The lower part of the figure is giving the misfit. Note the two white encircled points. They are representing the "centers" of the q-BWF functions. In general, the center of a BWF or q-BWF does not coincide with the position of the peak. "hwhm" means "half width at half maximum".

In the Figure 1, note please that the values of the two q-parameters are 1.54 and 1.77. The functions are far from being of the Gaussian type. The result shown in the Figure 1 is very good, and we have used only two components, that is two q-BWF functions. If we use two Gaussians or two q-Gaussians, we have a relevant misfit between the data and the sum of components. Then, we need more than two components to fit the profile. J1133 is considered by Kramer et al., 1994.

J1133—6250/1369 - <u>https://psrweb.jb.man.ac.uk/epndb/#jk17/J1133-6250/J1133-6250.1400MHz.psrfits</u>, EPN database under the Creative Commons Attribution 4.0 International license. Data are courtesy by Johnston and Kerr, 2018. Also in this case, let us use two q-BWF functions.
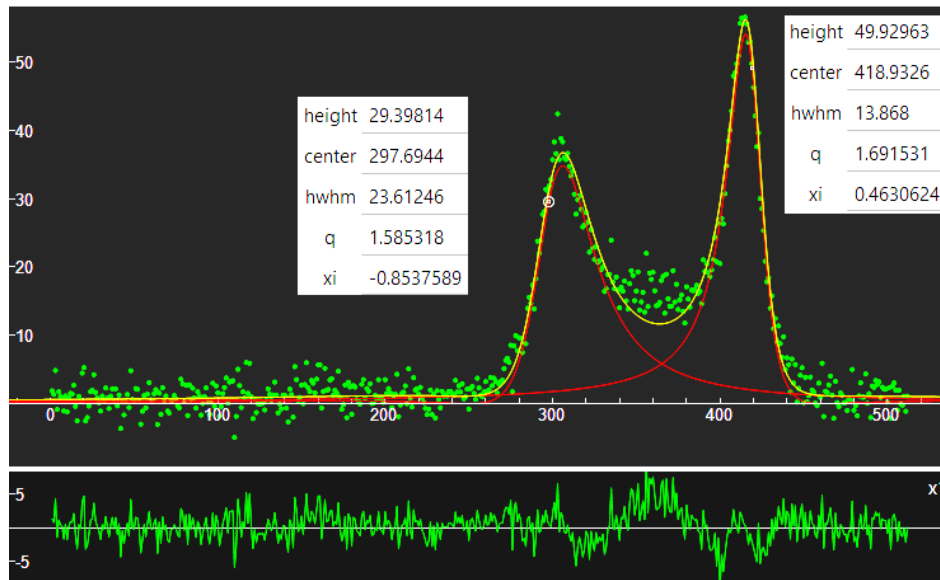
Fig. 2: The image is giving a screenshot of Fityk. The data are those of the pulsar profile
(black line). The parameters of the two used q-BWF components (red lines) are given in the figure. Note that the values of the q-parameters are indicating that the behavior of the functions is not a Gaussian one.
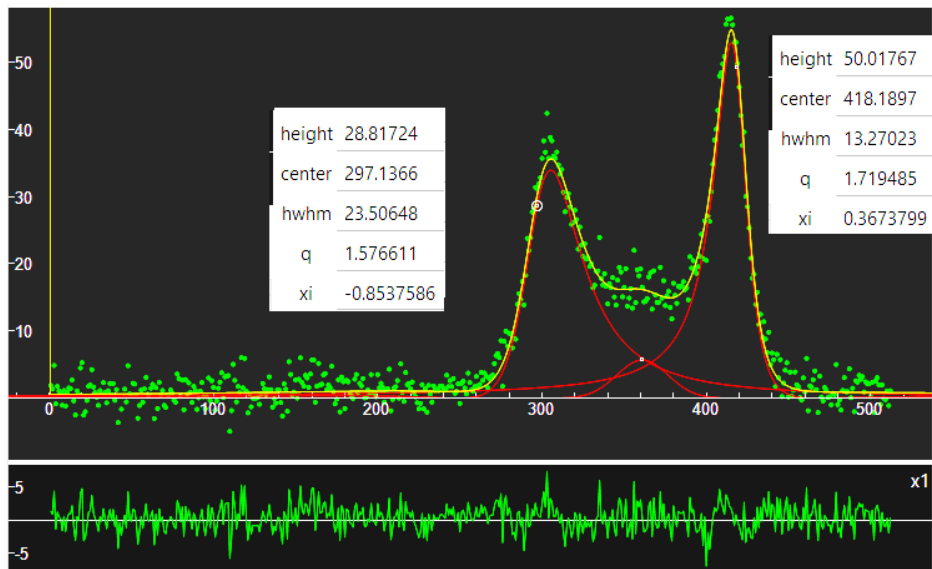

Fig. 3: Data as in the Fig.2. To the two q-Breit functions, a q-Gaussian is added between the peaks. The misfit is improved.

J1706-4310 - https://psrweb.jb.man.ac.uk/epndb/#kbm+03/J1706-4310/kbm+03_1374.epn, EPN database under the Creative Commons Attribution 4.0 International license. Data are a courtesy by Kramer et al., 2003. Let use two q-Gaussians. Here the result is given in the Fig.4.
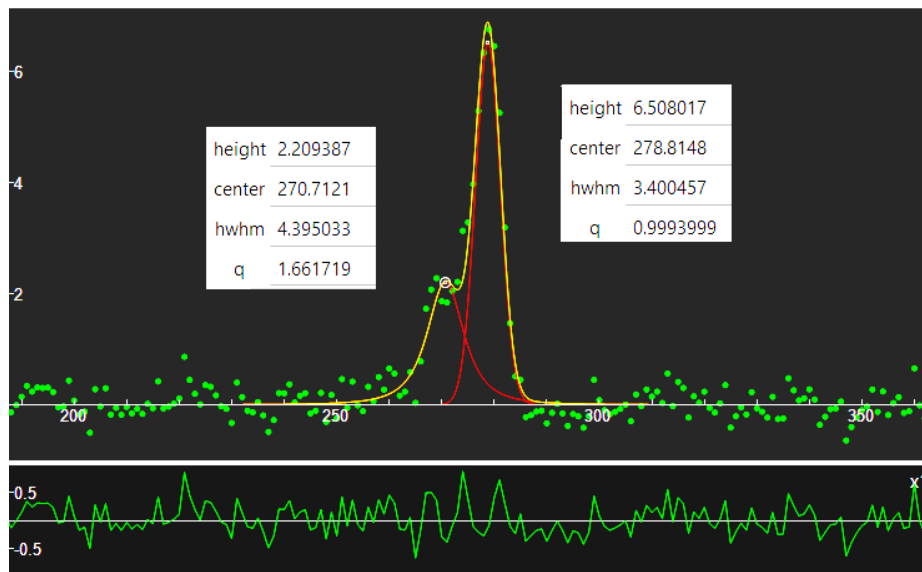
Fig. 4: The data are those of the pulsar profile https://psrweb.jb.man.ac.uk/epndb/#kbm+03/J1706-4310/kbm+03_1374.epn. The parameters of the two q-Gaussians are given in the figure. One, q=0.999, is indicating a Gaussian profile, whereas the other, q=1.662, is telling that the profile is intermediate between Lorentzian and Gaussian line shapes.

J1706-4310 - https://psrweb.jb.man.ac.uk/epndb/#kbm+03/J1706-3839/kbm+03_1374.epn, EPN database under the Creative Commons Attribution 4.0 International license. Data are a courtesy by Kramer et al., 2003. Also in this case, let us use two q-Gaussians as in the Figure 5.
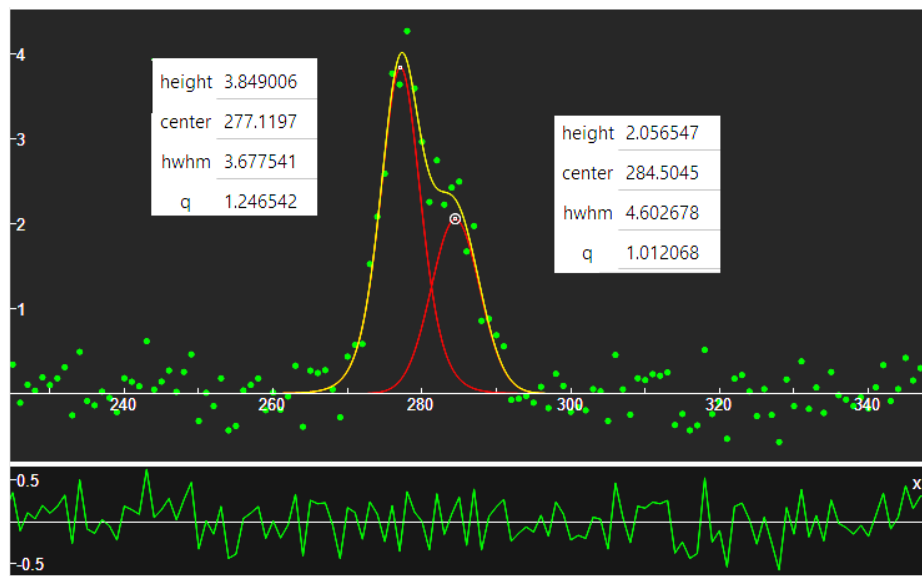

Fig. 5: The data are those of the pulsar profile https://psrweb.jb.man.ac.uk/epndb/#kbm+03/J1706-3839/kbm+03_1374.epn. The parameters of the two used q-Gaussian (red lines) are given in the figure. Note that, in this case, the q parameters are indicating Gaussian-like profiles.

J0435 - https://psrweb.jb.man.ac.uk/epndb/#bkk+16/J0435+2749/J0435+27_HBA_census.0000_0000.ar, EPN database under the Creative Commons Attribution 4.0 International license. Data are a courtesy by Bilous et al., 2016. In this case we have a large peak which seems being asymmetric.
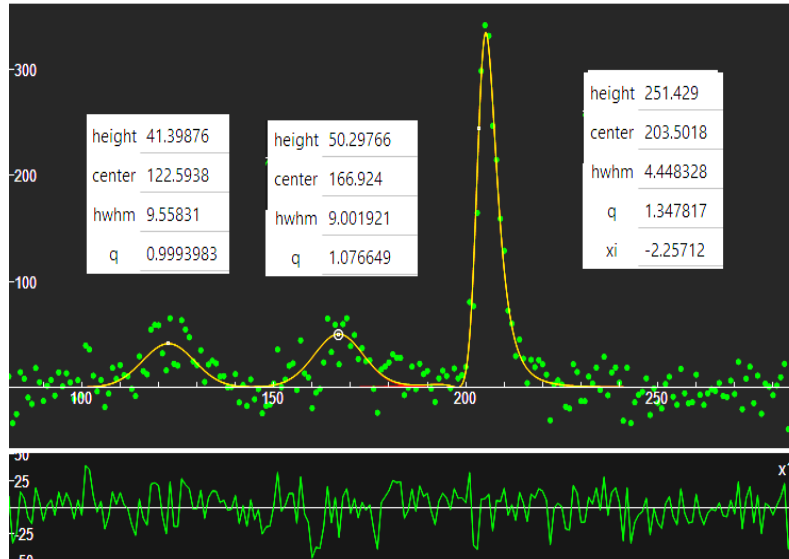

Fig. 6: Profile https://psrweb.jb.man.ac.uk/epndb/#bkk+16/J0435+2749/J0435+27_HBA_census.0000_0000.ar. A q-WBF function is used for the main component. Two further q-Gaussians are used as in the figure.

J0435 -, https://psrweb.jb.man.ac.uk/epndb/#wrvo23_b/J0435+2749/J0435+2749.53861ap0.asc, EPN database under the Creative Commons Attribution 4.0 International license. Data are a courtesy by Wahl et al., 2023.
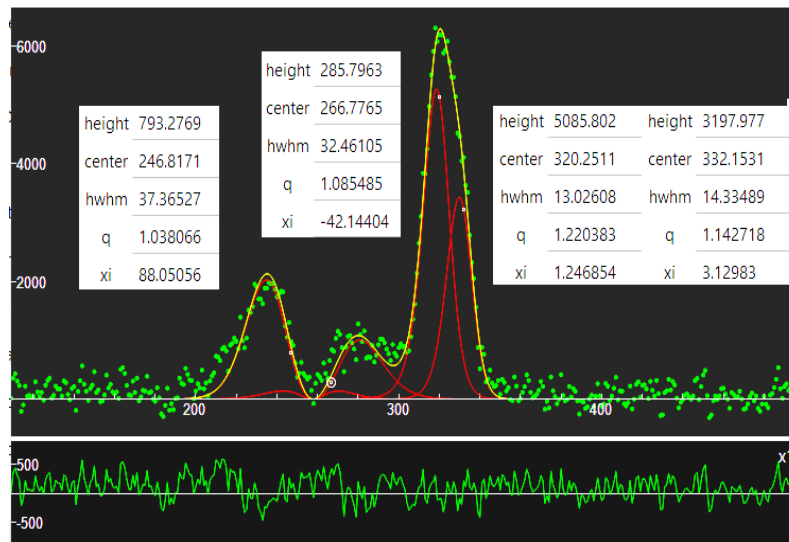
Fig. 7: The same pulsar of the Figure 6, but the profile is given by data https://psrweb.jb.man.ac.uk/epndb/#wrvo23_b/J0435+2749/J0435+2749.53861ap0.asc. Four q-BWF functions have been used, two are regarding the main peak (the related parameters are given on the right of the peak). Note that the values of the q-parameters are close to 1, so we have a Gaussian-like behavior. Therefore, let us try to fit the same data with four q-Gaussians. The result is given in the following Figure 8.

height	5800.828
center	319.1008
hwhm	8.83502
q	1.278113

height	2733.522
center	329.8651
hwhm	7.956887
q	1.158212

Fig. 8: The same data as Figure 7, https://psrweb.jb.man.ac.uk/epndb/#wrvo23_b/J0435+2749/J0435+2749.53861ap0.asc. Four q-Gaussians have been used. The parameters of the two components of the main peak are given in the figure. Note that the values of the q-parameters are very close to those given in the Figure 7.

J0435 - https://psrweb.jb.man.ac.uk/epndb/#wrvo23/J0435+2749/J0435+27.54541la0.asc, EPN database under the Creative Commons Attribution 4.0 International license. Data are a courtesy by Wahl et al., 2023.
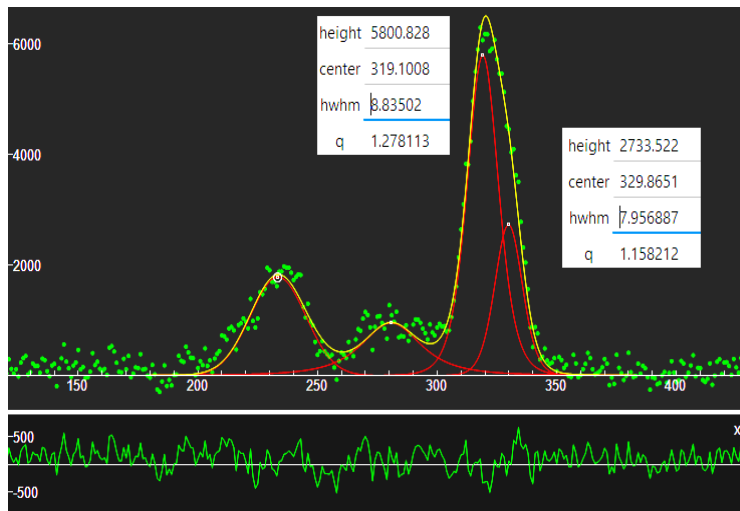

height	391.4591	height	143.2609	height	238.3351	height	335.0468	height	192.765
center	439.6174	center	478.733	center	548.3081	center	620.057	center	646.2863
hwhm	67.34621	hwhm	84.83126	hwhm	39.69482	hwhm	106.7713	hwhm	82.87725
q	1.014329	q	1.034363	q	1.141244	q	1.006887	q	1.00404
xi	-96.83697	xi	-27.21562	xi	1.348841	xi	281.8004	xi	748.2613

Fig.9: Five q-BWF functions for https://psrweb.jb.man.ac.uk/epndb/#wrvo23/J0435+2749/J0435+27.54541la0.asc
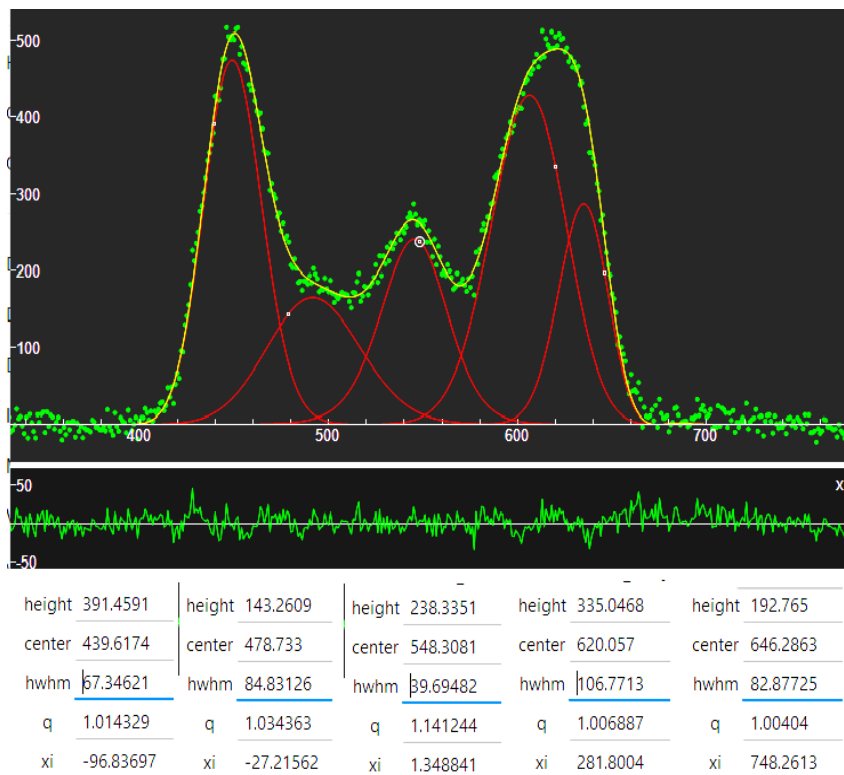
In the Figure 9, we have used five q-WBF functions. If we consider the q-parameters, we can see that they are close to the value 1. For this reason, let us fix the value of parameter *xi* to zero, in these five functions, and run the Fityk program again. We have the result given in the following Figure 10.
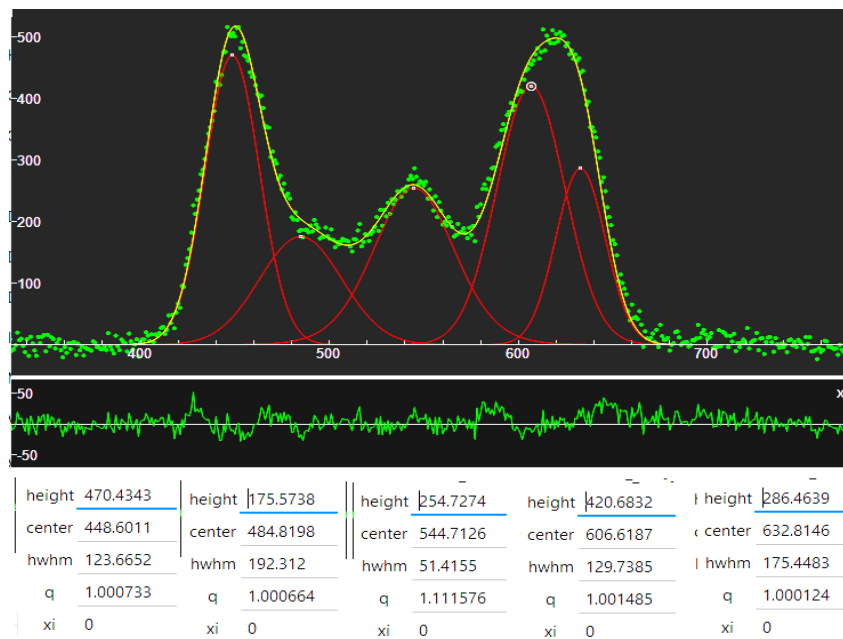

height	470.4343	height	175.5738	height	254.7274	height	420.6832	height	286.4639
center	448.6011	center	484.8198	center	544.7126	center	606.6187	center	632.8146
hwhm	123.6652	hwhm	192.312	hwhm	51.4155	hwhm	129.7385	hwhm	175.4483
q	1.000733	q	1.000664	q	1.111576	q	1.001485	q	1.000124
xi	0	xi	0	xi	0	xi	0	xi	0

Fig.10: The same as in the Figure 9, with five q-BWF functions with xi fixed to zero. That is, we are using five q-Gaussians.

Discussion

Figures 9 and 10 are very useful for a discussion concerning the q-BWF functions. As told in the caption of the Figure 1, the center of a q-BWF does not coincide with the position of the peak. The values of "height" and "hwhm", that is "half width at half maximum", are affected by the position of the center, as we can easily see comparing the parameters given in the Figs. 9 and 10. Therefore, the use of q-BWF functions is more complex than that of the q-Gaussians. However, as shown in the Figure 1, the q-BWF functions are able of fitting the profiles with a limited number of components. Further investigation is required, with a systematic analysis of EPN Database of Pulsar Profiles, to determine how many cases do require an approach with q-BWF asymmetric functions. Moreover, the values of the q-parameters can tell us if the pulsar profile features are close to being Gaussian or not.

Notes

About baselines. Only in the case of J1133-6250, a baseline of constant value 40183 has been subtracted from data. No other baseline correction has been applied.

The Fityk screenshots show the data as given in the files .txt. Therefore, on the x-axis we have integer values. In plots proposed by the EPN Database, a different scale is given. Accordingly, some processing has be done by the plotting tool. Let us compare the plot proposed by EPN Database and the plot of data from file .txt in the case of J0435, https://psrweb.jb.man.ac.uk/epndb/#wrvo23/J0435+2749/J0435+27.54541la0.asc. Using GIMP, the result of comparison is given in the following Figure 11a, where the black curve is representative for data as proposed by the EPN plot and the red curve the data from file .txt. We can see that have a shift. Accordingly, the superposition of the two curves is given in the Figure 11b. Differences are completely negligible.
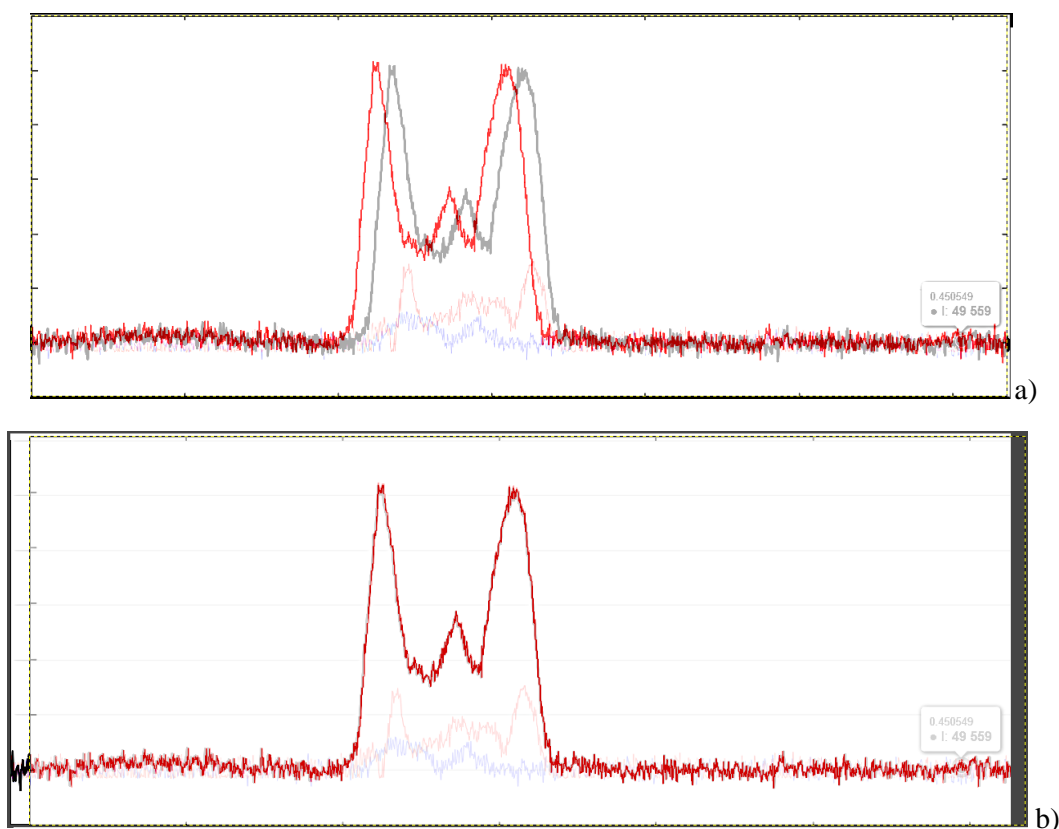
Fig. 11: Panel a): The black curve is representing the data as proposed by the EPN plot and the red curve the data from file .txt. Note the shift. Panel b): The two curves are superimposed.

Appendix – q-Gaussian, split-q-Gaussian and q-BWF functions

The q-Gaussian functions are probability distributions proper of the Tsallis statistics (Tsallis, 1988, Hanel et al., 2009). These functions are based on a generalized form of the exponential function, characterized by a continuous real parameter q. When q is going to 1, the q-exponential becomes the usual exponential function. The value q=2, (Naudts, 2009), corresponds to the Cauchy distribution, also known as the Lorentzian distribution; the q-Gaussian function is therefore a generalization of the Lorentzian distribution too. The change of q-parameter is allowing the q-Gaussian function to pass from the Gaussian to the Lorentzian distribution.

As given by Umarov et al., 2008, the q-Gaussian function is: $f(x) = Ce_q(-\beta x^2)$, where $e_q(.)$ is the q-exponential function and C a scale constant (in the exponent, $\beta = 1/(2\sigma^2)$). The q-exponential has expression: $e_q(u) = [1 + (1-q)u]^{1/(1-q)}$.

To have an asymmetric form of the q-Gaussian function, let us write it in the following manner (the center of the band is at x_o): $q\text{-}Gaussian(x) = Cexp_q(-\beta(x - x_o)^2) = C[1 - (1-q)\beta(x - x_o)^2]^{1/(1-q)}$

In [ChemRxiv](#) we considered the asymmetric q-Gaussians, as given by Devi (2021):

$q\text{-}Gaussian_L(x) = Cexp_{q_L}(-\beta_L(x - x_o)^2) = C[1 - (1-q_L)\beta_L(x - x_o)^2]^{1/(1-q_L)}$, when $x - x_0 < 0$

$q\text{-}Gaussian_R(x) = Cexp_{q_R}(-\beta_R(x - x_o)^2) = C[1 - (1-q_R)\beta_R(x - x_o)^2]^{1/(1-q_R)}$, when $x - x_0 > 0$

Parameters q and β of the Left and the Right parts are different. The most proper name for this asymmetric function is split-q-Gaussian. As previously shown, we have also generalized the Breit-Wigner-Fano into a [q-Breit-Wigner-Fano](#).

In Fityk, a q-Gaussian function can be defined in the following manner:

define Qgau(height, center, hwhm, q=1.5) = height*(1+(q-1)*((x-center)/hwhm)^2)^(1/(1-q))

q=1.5 the initial guessed value of the q-parameter. Parameter hwhm is the half width at half maximum of the component. When q=2, the q-Gaussian is a Lorentzian function, that we can find defined in Fityk as:

Lorentzian(height, center, hwhm) = height/(1+((x-center)/hwhm)^2)

When q is close to 1, the q-Gaussian becomes a Gaussian function. The split q-Gaussian is defined as:

Splitqgau(height, center, hwhm1=hwhm, hwhm2=hwhm, q1=1.5, q2=1.5) = x < center ? Qgau(height, center, hwhm1, q1) : Qgau(height, center, hwhm2, q2)

The split Lorentzian is: SplitLorentzian(height, center, hwhm1=hwhm, hwhm2=hwhm) = x < center ? Lorentzian(height, center, hwhm1) : Lorentzian(height, center, hwhm2)

And the q-BWF can be defined as:

Qbreit(height, center, hwhm, q=1.5, xi=0.1) = (1-xi*(q-1)*(x-center)/hwhm)^2 * height*(1+(q-1)^0.5 *((x-center)/hwhm)^2)^(1/(1-q))

And the BWF can be defined as:

Breit(height, center, hwhm, xi=0.1) = (1-xi*(x-center)/hwhm)^2 * height/(1+((x-center)/hwhm)^2)

Using +xi instead of -xi does not change the fitting results in Fityk.

Acknowledgement

References

1. Backer, D. C. (1975). Pulsar average waveforms and hollow cone beam models (No. X-693-75-138).

2. Beskin, V. S., Chernov, S. V., Gwinn, C. R., & Tchekhovskoy, A. A. (2015). Radio pulsars. Space Science Reviews, 191, 207-237. https://doi.org/10.1007/s11214-015-0173-8

3. Bianconi, A. (2003). Ugo Fano and shape resonances. In AIP Conference Proceedings (Vol. 652, No. 1, pp. 13-18). American Institute of Physics.

4. Bilous, A.V., Kondratiev, V.I., Kramer, M., Keane, E.F., Hessels, J.W.T., Stappers, B.W., Malofeev, V.M., Sobey, C., Breton, R.P., Cooper, S. and Falcke, H., 2016. A LOFAR census of non-recycled pulsars: average profiles, dispersion measures, flux densities, and spectra. Astronomy & Astrophysics, 591, p.A134.

5. Devi, S. (2021). Asymmetric Tsallis distributions for modeling financial market dynamics. Physica A: Statistical Mechanics and Its Applications, 578, 126109

6. Fano, U. (1961). Effects of configuration interaction on intensities and phase shifts. Physical review, 124(6), 1866.

7. Ferrari, A. C., & Robertson, J. (2000). Interpretation of Raman spectra of disordered and amorphous carbon. Physical Review B 61: 14095–14107.

8. Guojun, Q., Manchester, R. N., Lyne, A. G., & Gould, D. M. (1995). Polarization and Faraday rotation measurements of southern pulsars. Monthly Notices of the Royal Astronomical Society, 274(2), 572-588.

9. Han, J. L., & Manchester, R. N. (2001). The shape of radio pulsar beams. Mon. Not. R. Astron. Soc, 320, L35-

L40.

10. Hanel, R., Thurner, S., & Tsallis, C. (2009). Limit distributions of scale-invariant probabilistic models of correlated random variables with the q-Gaussian as an explicit example. The European Physical Journal B, 72(2), 263.

11. Harding, A. K. (2017). Pulsar emission physics: The first fifty years. Proceedings of the International Astronomical Union, 13(S337), 52-57.

12. Johnston, S., & Kerr, M. (2018). Polarimetry of 600 pulsars from observations at 1.4 GHz with the Parkes radio telescope. Monthly Notices of the Royal Astronomical Society, 474(4), 4629-4636.

13. Kramer, M., Wielebinski, R., Jessner, A., Gil, J. A., & Seiradakis, J. H. (1994). Geometrical analysis of average pulsar profiles using multi-component Gaussian FITS at several frequencies. I. Method and analysis. Astronomy and Astrophysics Suppl., Vol. 107, p. 515-526 (1994), 107, 515-526.

14. Kramer, M. (1994). Geometrical analysis of average pulsar profiles using multi-component Gaussian FITS at several frequencies. II. Individual results. Astronomy and Astrophysics Suppl., Vol. 107, p. 527-539 (1994), 107, 527-539.

15. Kramer, M., Bell, J.F., Manchester, R.N., Lyne, A.G., Camilo, F., Stairs, I.H., D'Amico, N., Kaspi, V.M., Hobbs, G., Morris, D.J. and Crawford, F., 2003. The Parkes Multibeam Pulsar Survey–III. Young pulsars and the discovery and timing of 200 pulsars. Monthly Notices of the Royal Astronomical Society, 342(4), pp.1299-1324.

16. Lyne, A. G., & Manchester, R. N. (1988). The shape of pulsar radio beams. Monthly Notices of the Royal Astronomical Society, 234(3), 477-508.

17. Meier, R. J. (2005). On art and science in curve-fitting vibrational spectra. Vibrational spectroscopy, 2(39), 266-269.

18. Naudts, J. (2009). The q-exponential family in statistical physics. Central European Journal of Physics, 7, 405-413.

19. Rankin, J. M. (1983). Toward an Empirical Theory of Pulsar Emission-Part Two-on the Spectral Behavior of Component Width. Astrophysical Journal, Vol. 274, NO. 1, P. 359, 1983, 274, 359.

20. Rankin, J. (2016). Observing the Plasma-physical Processes Behind Pulsar Radiation, Goddard Pulsar Workshop, June 2016, available https://fermi.gsfc.nasa.gov/science/mtgs/pulsar_mag/slides/Rankin.pdf

21. Rankin, J. (2022). Radio pulsar beam geometry at lower frequencies: bright sources outside the Arecibo sky. Monthly Notices of the Royal Astronomical Society, 514(3), 3202-3211.

22. Sparavigna, A. C. (2015). Recurrence plots of pulsar profiles. Philica, 533.

23. Sparavigna, A. C. (2023). q-Gaussian Tsallis Line Shapes and Raman Spectral Bands. Int. J. Sciences, 12(3), 27-40, 2023, http://dx.doi.org/10.18483/ijSci.2671 Available at SSRN: https://ssrn.com/abstract=4398623

24. Sparavigna, A. C. (2023). Asymmetric q-Gaussian functions generalizing the Breit-Wigner-Fano functions. Zenodo. https://doi.org/10.5281/zenodo.8356165

25. Sparavigna, A. C. (2024). The Fitted q-Gaussian Function, from Voigt Profile to Kubo Lineshape. International Journal of Sciences, 13(03), 1-16.

26. Sparavigna, A. C. (2023). SERS Spectral Bands of L-Cysteine, Cysteamine and Homocysteine Fitted by Tsallis q-Gaussian Functions. International Journal of Sciences, 12(09), 14-24.

27. Sparavigna, A. C. (2024). Graphene and Graphene Oxide (Raman Spectroscopy). ChemRxiv. doi:10.26434/chemrxiv-2024-86stv-v2

28. Tsallis, C. (1988). Possible generalization of Boltzmann-Gibbs statistics. Journal of statistical physics, 52, 479-487.

29. Umarov, S., Tsallis, C., Steinberg, S. (2008). On a q-Central Limit Theorem Consistent with Nonextensive Statistical Mechanics. Milan J. Math. Birkhauser Verlag. 76: 307–328. doi:10.1007/s00032-008-0087-y. S2CID

55967725.

30. Wahl, H., Rankin, J., Venkataraman, A., & Olszanski, T. (2023). Radio pulsar emission-beam geometry at low frequency: LOFAR High-Band Survey sources studied using Arecibo at 1.4 GHz and 327 MHz. Monthly Notices of the Royal Astronomical Society, 520(1), 314-321.

31. Wang, H.G., Pi, F.P., Zheng, X.P., Deng, C.L., Wen, S.Q., Ye, F., Guan, K.Y., Liu, Y. and Xu, L.Q., 2014. A Fan Beam Model for radio pulsars. I. observational evidence. The Astrophysical Journal, 789(1), p.73.

32. Wojdyr, M. (2010). Fityk: a general-purpose peak fitting program. Journal of Applied Crystallography, 43(5-1), 1126-1128.